A microfluidic mixing system for single-molecule measurements

Shawn H. Pfeil,[1] Charles E. Wickersham,[1] Armin Hoffmann,[2] and Everett A. Lipman[1]
[1]*Department of Physics, University of California, Santa Barbara, California 93106, USA*
[2]*Biochemisches Institut, Universität Zürich, Winterthurerstrasse 190, 8057 Zürich, Switzerland*

(Received 23 December 2008; accepted 7 April 2009; published online 14 May 2009)

This article describes the design and fabrication of a microfluidic mixing system optimized for ultrasensitive optical measurements. Channels are replica-molded in polydimethylsiloxane elastomer and sealed with fused-silica coverglass. The resulting devices have broad chemical compatibility and extremely low fluorescence background, enabling measurements of individual molecules under well-characterized nonequilibrium conditions. Fluid delivery and pressure connections are made using an interface that allows for rapid assembly, rapid sample exchange, and modular device replacement while providing access for high numerical aperture optics. © *2009 American Institute of Physics.* [DOI: 10.1063/1.3125643]

I. INTRODUCTION

Since their introduction by Austin and co-workers[1,2] in the late 1990s, microfabricated diffusive mixers have found application in a large and growing number of chemical and biochemical kinetics measurements.[3–7] Compared with stopped flow[8] and turbulent mixers,[9,10] these laminar-flow devices provide greater uniformity of, and control over, mixing conditions, and require only microscopic sample volumes.

During the same period, the inception and development of single-molecule fluorescence measurements[11–15] have made possible the observation of macromolecular properties and behavior formerly cloaked by ensemble averaging. Combination of these techniques[16–21] enables measurements under nonequilibrium conditions with single-molecule resolution. For example, transiently inhabited subpopulations can be identified, examined, and tracked in protein folding experiments.[16,19,20] This ability to extract new information from biochemical kinetics experiments using only microliters of sample is promising, but the application of single-molecule diffusive mixers has remained limited.

In this article, we describe a system designed to overcome many of the difficulties commonly encountered in single-molecule microfluidic measurements.

Mixing devices are replica-molded[22–24] from poly(dimethylsiloxane) elastomer, so that cleanroom processing is unnecessary after mold fabrication. The channel pattern is designed to provide complete mixing with minimal dead time prior to observation, subject to constraints imposed by the optical system. Channel impedances have been selected to allow a wide range of precisely controllable flow rates and mixing ratios with a simple pressure regulation system.

Once contact-bonded to fused-silica windows, devices with cast feedthroughs are mounted in a spring-loaded chip carrier containing integrated sample wells, eliminating the need for adhesives, punching, and needle insertion to attach pressure and fluid feeds. The chip carrier can be rapidly loaded into a pressure manifold that mounts directly onto a microscope. All connections to the chip carrier are made using face-type static O-ring seals, so pressure delivery fittings can remain in place while devices are exchanged. Sample wells in the chip carrier are accessible with the carrier mounted, and can be emptied or refilled without moving the device or undoing any connections.

Although this system is optimized for single-molecule measurements, these devices can, if a suitable window-bonding technique is used, be run at least an order of magnitude faster for ensemble measurements.

II. DEVICE REQUIREMENTS AND DESIGN

A. Mixer materials

A microfluidic device intended for use with single-molecule detection is subject to a number of inescapable requirements, chief among which is the need for extremely low background fluorescence. In earlier work,[16] channel patterns were fabricated directly in silicon, and anodic bonding[25] was used to seal a window over the channels. This method takes advantage of mature silicon fabrication technology and the strong seal formed in the bonding process. Unfortunately, it requires that the window be made of Pyrex (or a similar glass), which produces significant fluorescence background. Further disadvantages are that these devices must be fabricated in a cleanroom, and are permanently sealed, making cleaning and reuse impractical.

Among available transparent materials, fused silica stands out as the best choice for the device window. It is transparent from 180–2100 nm,[26–28] has broad chemical compatibility, does not affect polarization, is readily available in the appropriate thickness, has an index of refraction compatible with high numerical aperture water-immersion optics, and produces approximately one-tenth the fluorescence background of Pyrex.

In typical fluorescence measurements of untethered single molecules,[13–16,29,30] photons are collected as the sample molecule drifts (by diffusion, flow, or both) through a laser focus coincident with a confocal detection volume having dimensions on the order of 1 μm. A meaningful measurement, for example of a Förster resonance energy transfer

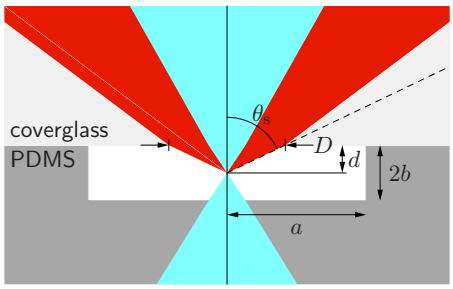

FIG. 1. (Color online) Laser beam and sample fluorescence in microfluidic channel. With the laser focus at depth d, the collected light cone will have diameter D at the top of the channel. $D=2Ad/\sqrt{n_s^2-A^2}$, where n_s is the index of refraction in the channel, and $A=n_s \sin \theta_s$ is the numerical aperture of the optical system used to collect the light. For $n_s=1.33$ and $A=1.2$, $D=4.18d$. Optimal measurements at the full depth $d=2b=10$ μm therefore require a channel width $2a \geq 41.8$ μm. In the present mixer design, $2a=50$ μm.

efficiency,[15] usually requires the detection of tens to hundreds of photons, corresponding to a dwell time in the focus on the order of 1 ms. For this reason, the flow velocity in the mixer's observation channel should not be significantly higher than 1 μm/ms (=1 mm/s). As a result of optical constraints (described below), the cross-sectional area of the observation channel is such that this maximum flow velocity is easily achieved with a driving pressure differential of less than 15 kPa.

This relatively low pressure requirement enables the use of poly(dimethylsiloxane) (PDMS) as the device substrate. With the exception of several narrow absorption bands in the near-infrared, PDMS is transparent from 240 to 2100 nm.[31,32] It is compatible with a wide range of laboratory chemicals,[33] suitable for biological samples,[34] and inexpensive. It also allows device fabrication using replica-molding methods introduced by Duffy, *et al.*[22] and developed by Whitesides and co-workers[23,31,33,34] and Quake and co-workers.[24,35] PDMS undergoes reversible conformal contact bonding with fused silica, forming a seal that is usable up to approximately 30 kPa.[36] Higher pressures, useful for ensemble experiments employing rapid flow, can be withstood by irreversible device-window seals formed using plasma, ultraviolet light, or additional PDMS.[22,37–39]

B. Observation channel

A microscope objective with numerical aperture $A \equiv n \sin \theta$ can collect a cone of light with half-angle θ, where n is the index of refraction of the medium in which θ is measured (see Fig. 1). Since typical fluorescence lifetimes are 10–100 times longer than rotational correlation times for freely diffusing molecules in aqueous solution, emission is expected to be isotropic. The cone will therefore contain a fraction

$$f_c = \tfrac{1}{2}(1-\cos\theta_s) = \tfrac{1}{2}[1-\sqrt{1-(A/n_s)^2}] \quad (1)$$

of the light emitted by a sample molecule, where θ_s is the cone half-angle at the sample, and n_s is the index of refraction in the observation channel (Although θ changes as the light cone propagates from one medium to another, A is invariant). For typical values $n_s=1.33$ and $A=1.2$, $\theta_s=64.5°$, and the collection efficiency $f_c=0.28$.

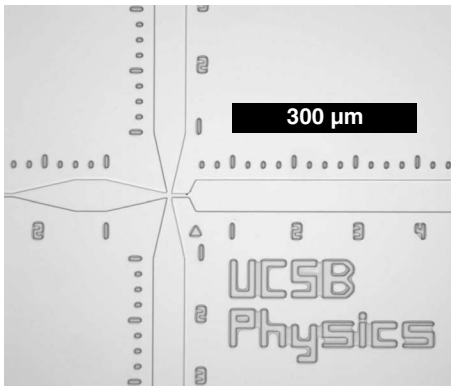

FIG. 2. Microfluidic device mixing region. Etched reference marks facilitate precise positioning of the confocal measurement volume. 50 μm wide areas are used for measurements in the inlet channels at top, left, and bottom. The first position where a measurement can be made using the entire collection cone of an objective with numerical aperture $A=1.2$ is indicated by a small triangle below the observation channel.

To prevent further loss of the already scarce signal from a single-molecule sample, microfluidic channels must be wide enough to accommodate the entire light cone originating at observation depth d (Fig. 1). At the level of the PDMS-coverglass interface, the cone diameter $D=2Ad/\sqrt{n_s^2-A^2}$. For the parameters given above, $D=4.18d$. If measurements are to be made down to the bottom center of an observation channel with depth $2b$ and width $2a$, the maximum numerical aperture that can be fully accommodated is $A_c=n_s/\sqrt{1+4(b/a)^2}$.

Single-molecule kinetic measurements made possible by this type of microfluidic mixer rely on the conversion between channel position and time using the flow rate in the device. To minimize measurement uncertainty, it is necessary to have a uniform flow profile throughout the confocal volume from which signal is being collected. The confocal volume has a vertical extent on the order of 1 μm, so the channel depth must be significantly greater than this to assure the desired flow uniformity.

A channel depth of 10 μm was chosen for the present mixer design. This is sufficient to ensure a velocity variation of no more than 1% over the 1×1 μm square area at the center of the channel cross section in fully developed flow.[40] Observations at the full depth with an $A=1.2$ water-immersion microscope objective (UPLSAPO 60XW, Olympus) then require that the channel be at least 41.8 μm wide (Fig. 1). Accordingly, the observation channel width was chosen to be 50 μm. Figure 2 shows the observation channel and 50 μm wide areas used for control measurements of sample and buffer prior to mixing.

C. Mixing performance and dead time

A perfect mixer would combine reactants completely and instantaneously, allowing observation of the sample from the moment of mixing onward. In realizable devices, departures from this ideal are described by a mixing delay and a measurement "dead time." How one defines these two quantities is somewhat arbitrary. For example, the driving pressure can always be increased, resulting in a higher flow rate and correspondingly lower dead time. For single-molecule

experiments, however, the amount of signal collected is reduced when the sample spends less time in the confocal volume, and at some point claims of extremely short dead times will become meaningless as the signal-to-noise ratio approaches zero. Likewise, measurements made prior to complete mixing of reactants are difficult or impossible to interpret.

1. Mixing delay

The dimensions of the channels in our microfluidic mixers are on the order of tens of microns, and the flow velocities (see Sec. II A above) are on the order of millimeters per second. Accordingly, for aqueous samples the Reynolds number[40,41]

$$R_e \equiv \frac{\rho U L}{\eta} \approx 10^{-2}, \tag{2}$$

where $\rho \approx 1000$ kg/m^3 is the density of water, U is the flow velocity, L is the channel dimension, and $\eta \approx 0.001$ Pa s is the viscosity of water. The transition to turbulent flow is not expected below $R_e \approx 2000$, so it is clear that flow in these mixers will be completely laminar, and mixing will be by diffusion alone.

In the experiment described in Ref. 16, protein molecules in a relatively high concentration of a denaturant, guanidinium chloride (GdmCl), were made to refold upon dilution of the denaturant. Dilution is complete once the denaturant molecules have had time to diffuse throughout the entire available post-mixing solution volume. In a symmetric planar mixer (Fig. 3) delivering a relatively large amount of buffer (side inlets), the sample solution (central inlet) is initially confined by hydrodynamic focusing[2] to a region near the horizontal center of the channel. Denaturant molecules with diffusion constant $\mathcal{D}$ will reach the sides of the channel in a time $\tau_m \approx a^2/2\mathcal{D}$, where a is the channel half-width (Fig. 1).

The present mixer (Fig. 3) was designed with a 5 μm wide neck following the mixing intersection, minimizing τ_m while keeping feature sizes well above the resolution limit (about 1 μm) of the fabrication process. For small molecules with $\mathcal{D} \approx 1$ μm^2/ms, we then have $\tau_m \approx 3$ ms. The average flow velocity U_m in the mixing neck will be ten times that in the 50 μm wide observation channel (the depth of all device features is 10 μm). The neck must therefore have a length $U_m \tau_m \approx 30$ μm for complete mixing.

Mixer parameters were tested and refined using numerical fluid flow calculations coupled with a Newtonian transport model for diffusion (OpenFOAM software, www.opencfd.co.uk). Figure 3(a) shows the result of a calculation with aqueous (η=1 mPa s) solutions in all three inlets and a small-molecule ($\mathcal{D}$=1 μm^2/ms) solute in the center inlet. For this calculation and the corresponding ink-mixing experiment [Fig. 3(b)], pressures at all three inlets were set to 12.4 kPa above that at the outlet. Under these conditions, the average flow velocity in the outlet channel is approximately 1.1 μm/ms. At the first observation point (see Fig. 2 caption), the velocity u_c of the central streamline is 4.3 μm/ms. Further down the observation channel, u_c approaches its asymptotic value of 1.8 μm/ms. In Fig. 3(a),

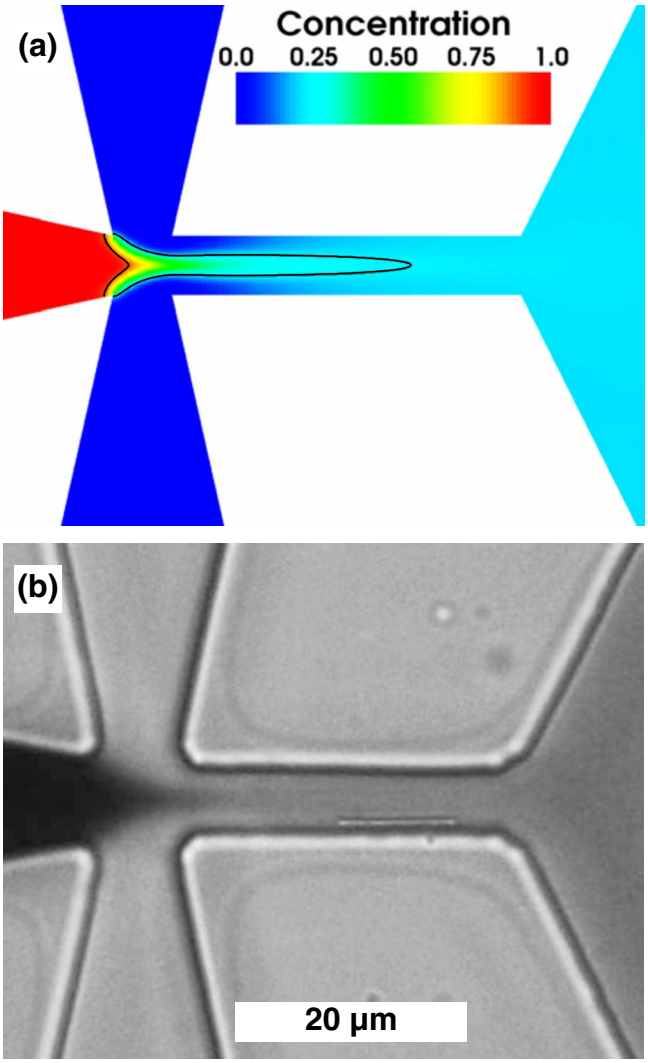

FIG. 3. (Color online) Numerical calculation of flow pattern and photograph of mixing region. Inlet channels narrow from observation areas (see Fig. 2) to an intersection followed by a 5 μm wide mixing channel. The mixing channel widens into the observation channel. (a) Calculation of ink concentration in the mixing pattern. Black lines are contours at 90% of the initial concentration and 110% of the final concentration. (b) Photograph of ink (Quink, Parker) mixing with water in the microfluidic device.

contour lines are drawn at 90% of the initial and 110% of the final solute concentrations. If we regard these lines as indicating the onset and completion of mixing (These choices are arbitrary, and the kinetics of a given sample may suggest different definitions for τ_m and dead time τ_d.), then we find a mixing delay τ_m=1.5 ms. Evidently this definition of τ_m makes the estimate $\tau_m \approx a^2/2\mathcal{D}$ rather conservative, as 110% of the final solute concentration is reached well before the mean-squared diffusion distance is half the channel width.

An average outflow velocity of 1 μm/ms results in a value of u_c too high for optimal single-molecule measurements, especially when, to minimize dead-time, observations must be made in a region where the central streamline is still decelerating. If the inlet pressures are reduced to 6.9 kPa, τ_m=2.2 ms, and at the first observation point u_c =2.4 μm/ms. Single-molecule measurements shown in Fig. 9 were made under these conditions at a point in the observation channel 100 μm downstream from the mixing inter-

TABLE I. Results of numerical mixing calculations (see text). Pressure P_i (relative to the outlet) is applied to the mixer inlets, resulting in mixing delay τ_m, dead time τ_d, and central streamline velocities u_{ci} at the first observation point and u_{cf} in the asymptotic fully developed flow. τ_m and τ_d are defined as the transit times from the 90% contour [see Fig. 3(a)] to the 110% contour and the first observation point (Fig. 2), respectively.

P_i (kPa)	τ_m (ms)	τ_d (ms)	u_{ci} (μm/ms)	u_{cf} (μm/ms)
20.2	1.8	1.8	7.0	3.0
12.4	1.5	3.1	4.3	1.8
6.9	2.2	6.3	2.4	1.0
4.0	4.4	11.7	1.4	0.61
3.0	8.0	18.9	1.0	0.44

section, where u_c had reached its asymptotic value of 1.0 μm/ms. Results from mixer calculations with various inlet pressures are summarized in Table I.

2. Dead time

In a planar mixing device optimized for optical single-molecule measurements, the confocal volume must be located at least half the channel-top light cone diameter ($D/2$ in Fig. 1) from any device wall in order to prevent occlusion of the fluorescence collected by the optical system. Since sample components must be separated by the device prior to mixing, $D/2$ is the minimum distance a mixed sample must travel before optimal observations can be made. The measurement dead time τ_d between the onset of mixing and the first observation is therefore constrained by this distance and the need to reduce u_c to a value on the order of 1 μm/ms (see Sec. II A) at the confocal volume.

With constant u_c, we would have $\tau_d \geq D/2u_c$, and typical values $u_c=1$ μm/ms, $d=5$ μm (Fig. 1), and $A=1.2$ would yield $D=20.9$ μm and $\tau_d \geq 10.5$ ms. In the present mixer design, the first measurement point (Fig. 2) is located well within the hydrodynamic entrance length[40] of the observation channel, so the fluid on the central streamline is decelerating as it passes through the confocal volume. If we define τ_d as the transit time from the 90% contour [see Fig. 3(a)] to the first measurement point, the calculation shown in Fig. 3(a) gives $\tau_d=3.1$ ms (see the second line in Table I). When the inlet pressures are reduced to 6.9 kPa, $\tau_d=6.3$ ms.

To set $u_c=1$ μm/ms at the first measurement point, the inlet pressures must be 3.0 kPa, and $\tau_d=18.9$ ms. Because of deceleration within the entrance length, the minimum dead time for an observation velocity $u_c=1$ μm/ms is obtained with the parameters shown on the fourth line of Table I. In this case, the optimal observation point is actually 4.9 μm beyond the first observation point, and the sample arrives there 16.1 ms after crossing the 90% contour [Note that we have defined τ_d as the time from the 90% contour to the first observation point (11.7 ms). The sample arrives at the first point where $u_c=1.0$ μm/ms in 16.1 ms.].

In ensemble experiments, or if one is willing to suffer loss of signal from single-molecule samples, τ_d can be reduced further by increasing the flow rate. It remains necessary to ensure that $\tau_d \geq \tau_m$. In the present mixer, the 110% contour coincides with the first measurement point ($\tau_d=\tau_m$) under the conditions shown in the first line of Table I.

The dead time limitation resulting from the optical configuration could possibly be overcome in multilayer devices by delivering the mixed sample to the confocal volume vertically.

D. Controllability

Flow in the microfluidic mixer is driven by a compressed air system (see Sec. II E), the resolution of which is limited to approximately 70 Pa (=0.01 PSI). So that the mixing pattern can be balanced, and the volume ratio of mixed fluids will be repeatable, it is necessary to have precise control over inlet flow rates. This can be achieved only if the mixer impedance is sufficient to prevent pressure changes on the order of the system resolution from having significant effects.

The combination of small dimensions and low fluid velocities ensures that flow in the mixer will be laminar (see Sec. II C 1). For channels with constant rectangular cross section, there will be a linear relationship between the driving pressure gradient dp/dx and the volume flow rate Q:[40]

$$Q = \left(-\frac{dp}{dx}\right)\frac{4ba^3}{3\eta}\left[1 - \frac{192a}{\pi^5 b}\sum_{k=1,3,5,\ldots}^{\infty}\frac{\tanh(k\pi b/2a)}{k^5}\right], \tag{3}$$

where flow is positive in the $+x$ direction, η is the fluid viscosity, a is the channel half-width, and b is the channel half-height (see Fig. 1). This equation can be recast in a form analogous to Ohm's law,[2]

$$Q = \Delta p/Z, \tag{4}$$

where Δp is the pressure drop along the length L of the channel ($dp/dx=-\Delta p/L$), and the flow impedance Z depends on L, a, b, and η.

For the observation channel (see Sec. II B) in the present mixer, $a=25$ μm, $b=5$ μm, and $L=11$ mm. With $\eta=1$ mPa s (water), the impedance $Z=3.0$ kPa s/nL. The average observation channel flow velocity $\bar{u}=Q/4ab$, so from Eq. (4), $\bar{u}=\Delta p/4abZ$. If we express Δp in kilopascals and Z in kPa s/nL, we have $\bar{u}=2.0\Delta p/Z=0.67\Delta p$ μm/ms. A fluctuation of 70 Pa in Δp would therefore change $\bar{u}$ by $0.67\times 0.07=0.05$ μm/ms, approximately 5% of the nominal observation channel velocity. Precise control over the fluid mixing ratio and outflow velocity clearly requires inlet channel impedances significantly larger than that resulting from the natural dimensions of the observation channel.

The present mixer was designed using the four-terminal lumped impedance model of Knight, *et al.*[2] [Fig. 4(a)]. Parameters were chosen to produce the conditions for a reference experiment in which a solution of protein in 7 M GdmCl denaturant ($\eta=1.92$ mPa s) is mixed with buffer ($\eta=1.0$ mPa s) at a ratio $Q_1/Q_4=0.1$ to initiate folding [It should be noted that in this experiment, rapid dilution, rather than mixing with a triggering reagent, is the goal. This is fundamentally different from the experiments of Knight, *et al.*[2] and similar subsequent work. Complete dilution requires that denaturant from the central inlet be distributed

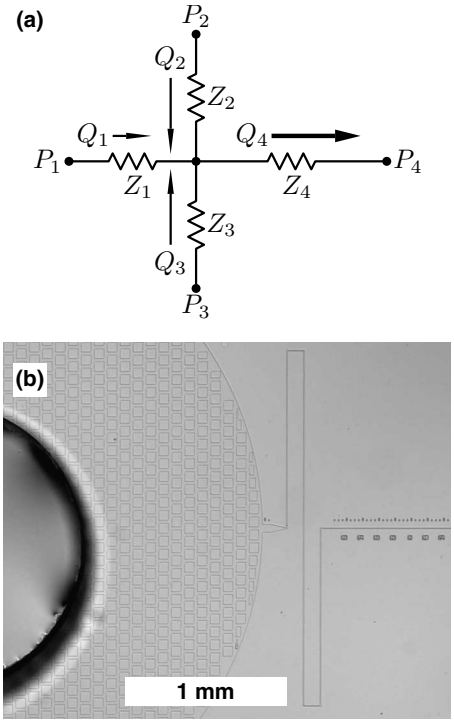

FIG. 4. (a) Four-terminal lumped impedance model used for device design (Ref. 2). Volume flow rates Q_i are proportional to pressure drops and inversely proportional to impedances Z_i, which for uniform rectangular channels are completely determined by fluid viscosity and channel dimensions. (b) Photograph of central inlet region. The fluid inlet, extending through the thickness of the device, is formed by casting to prevent rough edges and damage to the channel pattern. The PTFE post used for this purpose is centered within a large waffle-patterned pad (see text). The 5 μm wide central inlet channel is made to follow a serpentine path, increasing impedance and enabling precise control over flow rates and mixing.

uniformly throughout the entire post-mixing volume, and this must occur within the mixing neck, prior to observations. As shown in Fig. 3, denaturant concentration will have no significant variation across the channel width by the time sample solution enters the observation region (typical denaturant diffusion coefficients are similar to that of the ink seen in the figure).]. The observation channel average velocity is set to 1.0 μm/ms, and the nominal inlet pressures were chosen to be 12.4 kPa. The necessary impedances and resulting channel dimensions are shown in Table II. Tapered junctions and widened observation regions add on the order of 1% to the impedances shown, and have been neglected in the device design. Small pressure adjustments can be made if the design and/or fabrication do not provide sufficient precision for a particular experiment.

TABLE II. Channel dimensions and flow impedances. Values listed are for major segments of the mixer channels. Unlisted segments (tapers and premixing observation regions) add on the order of 1% to the tabulated inlet channel impedances. Impedances vary linearly with viscosity. Those shown here are calculated using η=1.0 mPa s (water). Dimensions a and b are shown in Fig. 1.

Channel	Z (kPa s/nL)	a (μm)	b (μm)	L (mm)
Central inlet	112	2.5	5	8.0
Side inlets	47	3	5	5.3
Mixing neck	0.42	2.5	5	0.030
Observation	3.0	25	5	11.0

Figure 4(b) shows extra length added to an inlet channel for increased impedance. Under the conditions of the design reference experiment, inlet flow rates can be controlled with a precision of approximately 0.6%.

Given a mixer with a predefined set of channel impedances, one can adjust the flow pattern by varying the inlet and outlet pressures. In this manner, a range of values can be chosen for the mixing ratio $m \equiv Q_1/Q_4$ [Fig. 4(a)] and the asymptotic central streamline velocity u_{cf} in the observation channel. Following Knight, *et al.*,[2] we consider a symmetric mixer for which the side inlet pressures $P_2=P_3=P_s$ and impedances $Z_2=Z_3=Z_s$. Analysis of the model yields

$$\frac{P_s - P_4}{P_1 - P_4} = \frac{1 + 2\sigma - m}{2(\sigma + \gamma m)}, \tag{5}$$

where $\sigma=Z_4/Z_s$ and $\gamma=Z_1/Z_s$. If the inlet pressures are made equal ($P_s=P_1$), Eq. (5) gives the natural mixing ratio for the device,

$$m_0 = \frac{1}{1 + 2\gamma}. \tag{6}$$

For the present mixer, m_0=0.17 for aqueous solutions (η =1.0 mPa s).

The selected value of m fixes the ratio of inlet pressures, leaving one degree of freedom by which u_{cf} may be adjusted,

$$P_1 - P_4 = \beta Z_s(\sigma + m\gamma)u_{cf}. \tag{7}$$

Here β is a geometry-dependent conversion factor between u_{cf} and the volume flow rate in the observation channel. For the observation channel described in Sec. II B, β =0.294 (nL/s)$\times$(μm/ms)$^{-1}$.

For a given set of channel impedances, pressures must be chosen so that flow is not reversed in the inlets or outlet.[2] Setting m=0 and m=1 in Eq. (5) gives

$$\frac{\sigma}{\sigma + \gamma} < \frac{P_s - P_4}{P_1 - P_4} < \frac{1 + 2\sigma}{2\sigma}. \tag{8}$$

Because of relatively low overall flow rates in single-molecule measurements, care must be taken to prevent premature mixing by diffusion into the inlet channels. This effect determines the usable lower bound on m in the present mixer, and is partly responsible for the increased values of τ_m and τ_d seen in the last line of Table I.

It should also be noted that diffusion will eventually erode the correspondence, initially provided by u_c, between position along the observation channel and time since mixing. Sample molecules will diffuse along the flow axis, and will arrive in the confocal volume after having explored slower off-axis streamlines. In the observation channel of the present mixer (Figs. 1 and 2), the sample distribution passes through a number of qualitatively different stages. Molecules in the central mixing jet first diffuse across the vertical extent of the channel ($t \approx b^2/2\mathcal{D}_s$, on the order of hundreds of milliseconds, where $\mathcal{D}_s$ is the sample diffusion constant), and later fill the entire channel ($t \approx a^2/2\mathcal{D}_s$, on the order of seconds). Eventually the solution reaches an asymptotic limit of uniform sample concentration across the observation channel

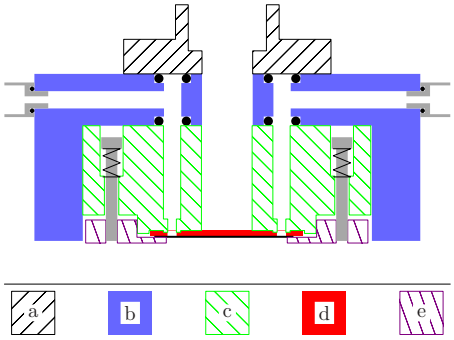

FIG. 5. (Color online) Interface cross section. (a) Removable pressure cap with optical port. (b) Aluminum pressure manifold. (c) PTFE chip carrier with sample wells. (d) PDMS microfluidic device bonded to coverglass. (e) Spring-loaded aluminum clamping plate. Screws holding the chip carrier in the manifold are not visible in this section.

cross section, and the arrival time distribution in any confocal volume will be very broad. If precise knowledge of this distribution is required, a careful analysis of the relationship between diffusion and the laminar flow profile must be carried out.[42]

E. Interface

The interface for the microfluidic mixer was developed with goals of precise flow control, access for high numerical aperture optics, broad chemical compatibility, and rapid exchange of both sample solutions and mounted mixing devices.

Fluid flow is driven by compressed air, which enables precise control over a wide range of flow rates on the order of nanoliters per second. The building compressed air supply (>1000 kPa) is passed through an in-line filter and reduced to 140 kPa using a general-purpose step-down regulator (Marsh-Bellofram Type 40, #960–065–000). The output of the step-down regulator supplies four precision mechanical regulators (Marsh-Bellofram Type 10LR, #960–053–000, 3.45–172 kPa range, 0.1% accuracy), each equipped with a digital pressure gauge (Cecomp Electronics DPG1000B5PSIG). Within the range from 3.5 to 34 kPa, the four pressure outputs can be adjusted with a precision of approximately 70 Pa, and an absolute accuracy, constrained by the gauges, of approximately 150 Pa.

The PDMS microfluidic mixer, bonded to a fused-silica coverglass, is clamped to a polytetrafluoroethylene (PTFE) chip carrier with integral sample wells (Figs. 5 and 6). Clamping force is provided by an adjustable spring-loaded anodized aluminum plate containing a window large enough to allow access by high numerical aperture microscope objectives. Raised circular bosses at the sample well outlets seal against the back side of the PDMS device, forming pressure-tight connections to the fluid inlet holes [Fig. 4(b)].

The chip carrier is mounted in an anodized aluminum pressure manifold, and connected using face-type static O-ring seals. Once the mixer and interface are in place on a microscope (Fig. 7), the removable pressure cap allows fluids to be placed directly in the sample wells using gel-loading pipette tips. With the cap in place, pressure from the regulators, delivered via tubing connectors on the sides of the manifold (Figs. 5 and 7), can be applied to the sample wells.

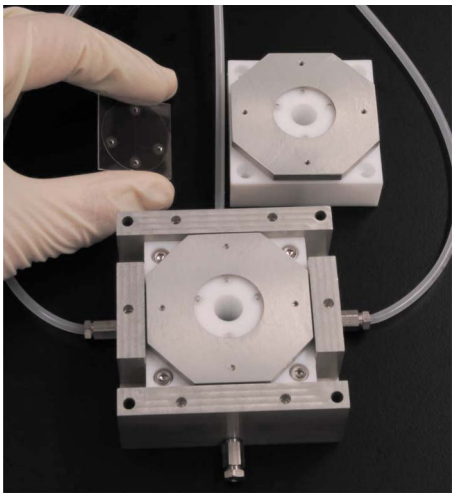

FIG. 6. (Color online) Assembled microfluidic mixing system (compare to Fig. 5). A microfabricated PDMS device, bonded to a fused-silica coverslip, is held against the PTFE chip carrier by a spring-loaded clamping plate. A large window in the clamping plate allows access for a microscope objective with high numerical aperture. Raised bosses around the chip carrier sample well outlets form seals with the inlets on the back side of the mixing device. Face-type static O-ring seals (Fig. 5) allow chip carriers with mounted devices to be rapidly swapped into and out of the aluminum pressure manifold.

A port, extending through the pressure cap, manifold, and chip carrier, enables illumination and observation of the back side of the mixer. Chip carriers, manifolds, pressure caps, and clamping plates were fabricated using a numerically controlled milling machine.

III. DEVICE FABRICATION

Device fabrication consists of four steps: generation of the mixer pattern, creation of a microfabricated mold in silicon, replica molding of PDMS devices, and final assembly.

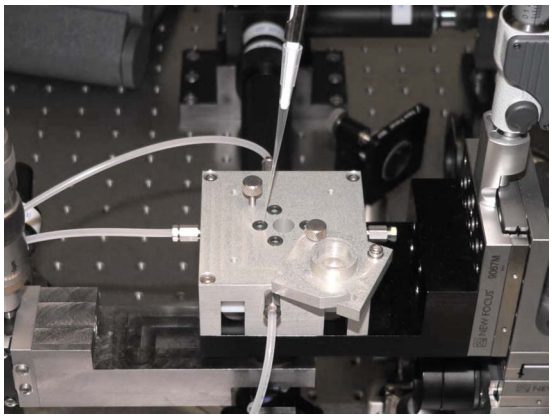

FIG. 7. (Color online) Mixing system mounted on single-molecule instrument. The removable pressure cap enables sample exchange using gel-loading pipette tips. Tubing connected to the aluminum manifold delivers precision-regulated compressed air for driving flow in the microfluidic mixer. The microscope objective (not visible) screws into the stainless steel beam below and to the left of the mixing system.

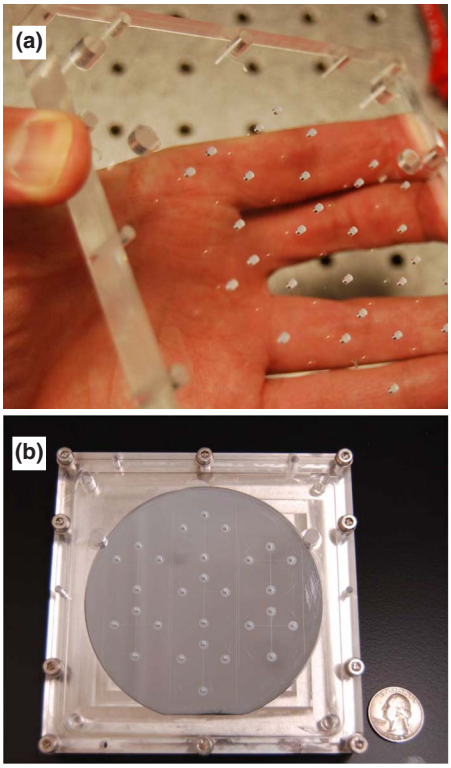

FIG. 8. (Color online) Composite casting dish. (a) PTFE posts embedded in the lid are used to cast smooth fluid inlets through the PDMS devices. (b) Complete casting assembly. When the lid is screwed down, inlet posts make firm contact with the silicon wafer. PDMS flows into the mold through holes near lid corners. The current design fits seven 27×27 mm^2 devices on a 100 mm diameter silicon wafer.

A. Mask generation

The channel pattern is drawn using computer-aided design software (DesignCAD, IMSI Design), and exported to a mask writer (DWL 66, Heidelberg Instruments) in DXF format. The pattern is written in AZ1518 (AZ Electronic Materials, Branchburg, NJ) photoresist on a chrome-plated soda-lime glass blank (Nanofilm Inc., Westlake Village, CA). Exposed photoresist is selectively removed with a 1:4 dilution of AZ400K developer in de-ionized water, and the remaining photoresist is used as a chemical etch mask for the chrome coating.

B. Silicon master creation

Masters for replica-molding must have their channel patterns aligned with the casting dish and lid (Fig. 8) in order to ensure proper placement of fluid inlets. Prior to photolithography, silicon wafers are screwed down into a form-fitting indentation in the casting dish, and reference marks are diamond-scribed on the wafers using a guide that is mechanically aligned with the dish.

After they are scribed, the wafers are immersed in piranha solution (1:5 v/v 30% hydrogen peroxide in concentrated sulfuric acid at 120 °C) for 20 min, thoroughly rinsed with de-ionized water, blown dry with nitrogen, and baked at 200 °C for 10 min to remove residual water.

Scribed and cleaned wafers are spin-coated with AZ5214-IR photoresist at 4000 RPM for 30 s, then soft-baked on a 95 °C hot plate for 60 s. A mask aligner (MA6, Karl Suss) is used to match scribed reference marks with corresponding marks in the chrome mask pattern, and the photoresist is exposed through the mask with 75 mJ/cm^2 of mercury I-line UV light.

Wafers and resist are given a post-exposure bake at 110 °C for 60 s, followed by a 450 mJ/cm^2 flood exposure. The photoresist is developed in a 1:4 dilution of AZ400K in de-ionized water for 45 s. Remaining photoresist, corresponding to the initial UV exposure pattern, is hardened at 200 °C for 10 min, removing any residual solvents in the process.

Bosch-process[43] deep reactive-ion etching was performed with an inductively coupled plasma system (Plasma-Therm 770) until the pattern depth reached 10 μm (approximately 8 min). Side-wall scalloping was negligible compared with channel dimensions. Feature heights were verified using a profilometry system (Dektak IIA, Veeco) prior to casting.

C. Device casting

In order to prevent PDMS adhesion, the silicon master must be chemically treated. The etched wafer is cleaned in piranha solution (see above) to remove residual photoresist, rinsed in distilled water, blown dry, and dehydrated at 200 °C for 10 min. Prior to each casting, the wafer is placed in a sealed Petri dish with a drop of trimethyl chlorosilane (TMCS) for 1 h. Because of its high vapor pressure, TMCS fills the reaction container. It reacts with the native silicon oxide layer on the wafer, coating the exposed surface with methyl groups that do not bond to PDMS as the oxide layer would.[44] This and all subsequent casting and assembly procedures can be performed outside of a cleanroom environment.

Following TMCS treatment, the patterned wafer is placed into a form-fitting cutout in the stainless steel casting dish [Fig. 8(b)], and held down with nylon screws. The depth of the cutout is such that after assembly, a 1 mm gap, defining the device thickness, is left between the top of the wafer and the bottom of the lid.

The casting assembly lid [Fig. 8(a)] is machined from clear acrylic. PTFE posts, cut from 1.6 mm diameter cord stock (McMaster-Carr Supply Co.), are embedded in milled holes that match fluid inlet positions on the wafer. When screwed down to the dish, the lid forces the posts into conformal contact with the wafer. Resulting smooth-edged fluid feeds in the cast devices eliminate the need for punching, which could damage or block the relatively shallow channels in the mixing devices. To minimize alignment problems, the silicon mold is designed with waffle-pattern inlet pads several millimeters in diameter [Fig. 4(b)]. The channels in the pattern have a relatively small width-to-height aspect ratio, which prevents collapse of the elastomeric device onto the coverglass. In addition, large particles in the incoming fluid are trapped, and a low-impedance path from the fluid inlet to the channel is ensured.

For casting, ten parts by weight of PDMS (RTV615, General Electric) are mixed with one part of crosslinking agent. The mixture is stirred for 5 min, then degassed in a vacuum desiccator for 40 min. Air is frequently bled into the desiccator to break bubbles. Degassed PDMS is slowly

poured through a 4 mm diameter funnel into a hole near the corner of the casting assembly lid [Fig. 8(b)], allowing most remaining air bubbles to float to the surface rather than entering the assembly. Once the mold is filled, the assembly is placed on an 80 °C hot plate to cure for 5 h.

After curing is completed, the lid is removed and individual devices are diced in place using a scalpel guided by etched borders on the wafer. Devices are left on the mold until they are mounted in order to minimize exposure of channel surfaces to airborne dust. For repeatable damage-free removal, a spatula-tipped tweezer is used to lift a few millimeters of the device around its entire perimeter, after which it is slowly peeled away from the wafer. Tweezer contact with patterned areas of the device must be avoided to prevent contamination.

D. Device assembly

The fourth wall of the cast microfluidic channels is provided by a fused-silica coverglass (see Sec. II A). Untreated PDMS is hydrophobic, which can make micron-scale channels difficult to fill with aqueous solutions. Pretreatment of the coverglass with piranha solution (see Sec. III B) or air plasma will remove fluorescent contaminants and make a sufficient fraction of the channel surface hydrophilic to enable low-pressure device loading.

For conformal contact bonding (Sec. II A), the coverglass (e.g., R425000, www.escoproducts.com) is cleaned with piranha solution as described in Sec. III B, rinsed in distilled water, and blown dry. It is then immediately brought into contact with the PDMS portion of the device. After use, the PDMS can be peeled off and discarded, allowing reuse of the relatively expensive fused-silica coverglass.

If high driving pressures (High-speed ensemble measurements in the microfluidic mixer can be compared with, for example, data from a commercial stopped-flow system.) or sample solutions that disrupt noncovalent contact bonding are to be used, a permanent PDMS-coverglass bond can be made using an air or oxygen plasma.[22] In this case, the coverglass is mechanically cleaned sequentially with detergent, acetone, isopropanol, and distilled water, blown dry, and exposed to plasma for 10 min (18 W at 10 MHz as produced in 40 Pa of air by a Harrick PDC-32G plasma cleaner). The coverglass is then mechanically cleaned with methanol to remove any remaining residue, and stored under distilled water to prevent contamination. Prior to bonding, the coverglass is blown dry and returned to the plasma cleaner along with a PDMS device placed so that the channels are exposed. The cleaner is then run with 40 Pa air at 7 W for 20 s. The plasma-treated sides of the coverglass and PDMS device are immediately brought into contact, and air bubbles are removed by applying light pressure with a cleanroom swab. Bonded devices can typically be used 1 h after assembly.

IV. SINGLE-MOLECULE DETECTION

Single-molecule measurements in the microfluidic mixer were performed using a custom-designed modular confocal microscope[29,30] (Fig. 7). A 488 nm continuous-wave laser (Coherent Sapphire) was reduced to 145 μW using absorptive neutral density filters, and focused in the observation channel using a water immersion microscope objective (Olympus UPLSAPO 60XW, 60×, $A=1.2$). The focal volume was placed at the center of the observation channel (as shown in Fig. 1) using reflections from the coverglass-water and water-PDMS interfaces.

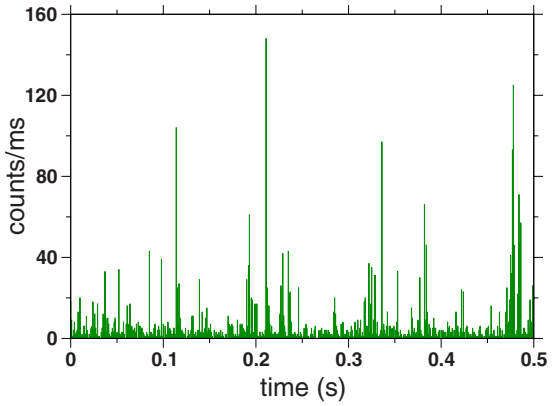

FIG. 9. (Color online) Fluorescence measurement in the microfluidic mixer. Single-molecule bursts are seen as a 15 pM solution of Alexa Fluor 488 hydrazide dye in distilled water flows through the confocal detection volume at the center of the observation channel. The solution is fed into all three inlets at a pressure of 6.9 kPa with respect to the outlet. Under these conditions, the flow velocity at the confocal volume, located 100 μm downstream from the mixing intersection, is 1.0 mm/s (=1.0 μm/ms). The measured background level is 1.1 ms^{-1}.

A 15 pM solution of Alexa Fluor 488 hydrazide dye (Invitrogen-Molecular Probes) in distilled water was delivered at 6.9 kPa to all three mixer inlets. The resulting asymptotic central streamline velocity in the observation channel was 1.0 μm/ms. The focal volume was placed in the fully developed flow 100 μm downstream from the mixing region.

Fluorescence from individual molecules passing through the focal volume was collected by the same objective used for excitation, and passed through an excitation beamsplitter (Omega 505DRLP, XF2010), tube lens, long-pass filter (Omega 493AELP, XR3000), and 100 μm confocal pinhole. The remaining signal was then reflected from a second dichroic beamsplitter (Omega 560DCLP, XF2016), filtered one last time (Chroma D525/50m), and focused on a photon-counting avalanche photodiode detector (PerkinElmer SPCM-AQR-16). Pulses from the detector module were collected by a 100 ps time digitizer (Ortec 9353), and photon arrival times were stored on a computer.

Data gathered into 1 ms bins are shown in Fig. 9. Single-molecule events are clearly visible, and the fluorescence background level (Background levels were determined by using parabolic fits to the peaks of the binned-signal histograms.) is 1.1 ms^{-1}. For the largest events, the signal-to-noise ratio exceeds 100 in 1 ms. Background levels in previous experiments[16] were 3–10 times higher, depending on the detection wavelength.

V. OUTLOOK

Although designed with protein folding experiments in mind, the microfluidic mixing system we have described is

flexible, and well-suited to a wide variety of measurements requiring rapid mixing and ultrasensitive light detection. In some applications, this technology will be able to replace conventional methods requiring sample volumes many orders of magnitude larger. For example, measurements of the firefly luciferin-luciferase reaction and its kinetics (to be published elsewhere) can be made with approximately one thousandth the sample volume used in a typical luminometer.

The device fabrication method and interface presented here will readily accommodate new mixer designs. Incorporation of sophisticated fluid handling[24,45] and three-dimensional fabrication can be expected to enhance the performance and utility of high-sensitivity optical measurements in future microfluidic mixers.

ACKNOWLEDGMENTS

We thank Benjamin Schuler for extensive testing of the microfluidic system and many valuable suggestions. We thank David Wood, Andrew Cleland, Stephen Quake, and Todd Squires for enlightening discussions and suggestions. Support for this work was provided by the Human Frontier Science Program and the DMEA Center for Nanoscience Innovation for Defense. A portion of this work was done in the UCSB nanofabrication facility, part of the NSF-funded NNIN network. E.A.L. is an Alfred P. Sloan research fellow.

[1] J. P. Brody, P. Yager, R. E. Goldstein, and R. H. Austin, Biophys. J. **71**, 3430 (1996).
[2] J. B. Knight, A. Vishwanath, J. P. Brody, and R. H. Austin, Phys. Rev. Lett. **80**, 3863 (1998).
[3] S. A. Pabit and S. J. Hagen, Biophys. J. **83**, 2872 (2002).
[4] D. E. Hertzog, X. Michalet, M. Jager, X. X. Kong, J. G. Santiago, S. Weiss, and O. Bakajin, Anal. Chem. **76**, 7169 (2004).
[5] M. B. Kerby, J. Lee, J. Ziperstein, and A. Tripathi, Biotechnol. Prog. **22**, 1416 (2006).
[6] D. J. Bornhop, J. C. Latham, A. Kussrow, D. A. Markov, R. D. Jones, and H. S. Sorensen, Science **317**, 1732 (2007).
[7] H. Y. Park, S. A. Kim, J. Korlach, E. Rhoades, L. W. Kwok, W. R. Zipfell, M. N. Waxham, W. W. Webb, and L. Pollack, Proc. Natl. Acad. Sci. U.S.A. **105**, 542 (2008).
[8] B. Chance, Rev. Sci. Instrum. **22**, 619 (1951).
[9] P. Davidovits and S. C. Chao, Anal. Chem. **52**, 2435 (1980).
[10] P. Regenfuss, R. M. Clegg, M. J. Fulwyler, F. J. Barrantes, and T. M. Jovin, Rev. Sci. Instrum. **56**, 283 (1985).
[11] E. B. Shera, N. K. Seitzinger, L. M. Davis, R. A. Keller, and S. A. Soper, Chem. Phys. Lett. **174**, 553 (1990).
[12] T. Ha, T. Enderle, D. F. Ogletree, D. S. Chemla, P. R. Selvin, and S. Weiss, Proc. Natl. Acad. Sci. U.S.A. **93**, 6264 (1996).
[13] S. Weiss, Science **283**, 1676 (1999).
[14] C. Zander, J. Enderlein, and R. A. Keller, *Single Molecule Detection in Solution* (Wiley, Berlin, 2002).
[15] C. Gell, D. Brockwell, and A. Smith, *Handbook of Single Molecule Fluorescence Spectroscopy* (Oxford University, Oxford, 2006).
[16] E. A. Lipman, B. Schuler, O. Bakajin, and W. A. Eaton, Science **301**, 1233 (2003).
[17] P. S. Dittrich, B. Muller, and P. Schwille, Phys. Chem. Chem. Phys. **6**, 4416 (2004).
[18] P. S. Dittrich and A. Manz, Anal. Bioanal. Chem. **382**, 1771 (2005).
[19] S. S. White, S. Balasubramanian, D. Klenerman, and L. M. Ying, Angew. Chem., Int. Ed. **45**, 7540 (2006).
[20] K. M. Hamadani and S. Weiss, Biophys. J. **95**, 352 (2008).
[21] D. Liao, P. Galajda, R. Riehn, R. Ilic, J. L. Puchalla, H. G. Yu, H. G. Craighead, and R. H. Austin, Opt. Express **16**, 10077 (2008).
[22] D. C. Duffy, J. C. McDonald, O. J. A. Schueller, and G. M. Whitesides, Anal. Chem. **70**, 4974 (1998).
[23] Y. N. Xia and G. M. Whitesides, Angew. Chem., Int. Ed. **37**, 550 (1998).
[24] M. A. Unger, H. P. Chou, T. Thorsen, A. Scherer, and S. R. Quake, Science **288**, 113 (2000).
[25] M. Elwenspoek and H. Jansen, *Silicon Micromachining* (Cambridge University, Cambridge, 1998).
[26] P. S. Shaw, K. R. Lykke, R. Gupta, T. R. O'Brian, U. Arp, H. H. White, T. B. Lucatorto, J. L. Dehmer, and A. C. Parr, Appl. Opt. **38**, 18 (1999).
[27] N. Neuroth, in *The Properties of Optical Glass*, edited by H. Bach and N. Neuroth (Springer, Berlin, 1995), Chap. 2, pp. 82–96.
[28] S. G. Kaplan, L. M. Hanssen, E. A. Early, M. E. Nadal, and D. Allen, Metrologia **39**, 157 (2002).
[29] B. Schuler, E. A. Lipman, and W. A. Eaton, Nature (London) **419**, 743 (2002).
[30] B. Schuler, E. A. Lipman, P. J. Steinbach, M. Kumke, and W. A. Eaton, Proc. Natl. Acad. Sci. U.S.A. **102**, 2754 (2005).
[31] J. C. McDonald and G. M. Whitesides, Acc. Chem. Res. **35**, 491 (2002).
[32] D. K. Cai, A. Neyer, R. Kuckuk, and H. M. Heise, Opt. Mater. (Amsterdam, Neth.) **30**, 1157 (2008).
[33] J. N. Lee, C. Park, and G. M. Whitesides, Anal. Chem. **75**, 6544 (2003).
[34] S. K. Sia and G. M. Whitesides, Electrophoresis **24**, 3563 (2003).
[35] H. P. Chou, C. Spence, A. Scherer, and S. Quake, Proc. Natl. Acad. Sci. U.S.A. **96**, 11 (1999).
[36] J. C. McDonald, D. C. Duffy, J. R. Anderson, D. T. Chiu, H. K. Wu, O. J. A. Schueller, and G. M. Whitesides, Electrophoresis **21**, 27 (2000).
[37] K. Haubert, T. Drier, and D. Beebe, Lab Chip **6**, 1548 (2006).
[38] L. Chen, J. C. Ren, R. Bi, and D. Chen, Electrophoresis **25**, 914 (2004).
[39] S. Satyanarayana, R. N. Karnik, and A. Majumdar, J. Microelectromech. Syst. **14**, 392 (2005).
[40] F. White, *Viscous Fluid Flow*, 2nd ed. (McGraw Hill, Boston, Massachusetts, 1991).
[41] T. M. Squires and S. R. Quake, Rev. Mod. Phys. **77**, 977 (2005).
[42] R. Mauri and S. Haber, SIAM J. Appl. Math. **51**, 1538 (1991).
[43] F. Laermer and A. Schlip, *Method of Anisotropically Etching Silicon*, U.S. Patent No. 5501893 (1996).
[44] S. Biggs and F. Grieser, J. Colloid Interface Sci. **165**, 425 (1994).
[45] J. Melin and S. R. Quake, Annu. Rev. Biophys. Biomol. Struct. **36**, 213 (2007).